

Gold Nanoparticles Stabilized by Tripod Thioether Oligomers: Synthesis and Molecular Dynamics Studies

Youichi Hosokawa,[1] Suguru Maki,[1] and Toshi Nagata*[,1,2]

[1]Institute for Molecular Science, 5-1 Higashiyama, Myodaiji, Okazaki 444-8787

[2]Department of Structural Molecular Science, The Graduate University for Advanced Studies, 5-1 Higashiyama, Myodaiji, Okazaki 444-8787

Received June 2, 2005; E-mail: toshi-n@ims.ac.jp

Gold nanoparticles (1.5–1.7 nm) were prepared by use of three tripod thioether oligomers as stabilizing molecules. The particle sizes were independent of the sizes of the stabilizers, and were smaller than those stabilized with simpler thioethers. Molecular dynamics simulations were performed to examine how the stabilizers adsorb on the nanoparticles. Parameters were developed for modeling the interactions between gold and organic molecules. Simulations in explicit chloroform solvent at 300 K revealed multiple-point adsorption of the stabilizers on the nanoparticles.

Recently, metal nanoparticles have received much attention as potentially useful materials[1] showing novel electronic properties derived from the quantum size effects,[2] as well as interesting catalytic reactivities.[3] The pioneering work of Brust[4] opened the field of monolayer protected gold nanoparticles,[5] which exhibit excellent stability and tractability in organic solvents. These materials are so stable that even chemical transformations of the pendant functional groups are possible through usual techniques of organic syntheses.[6] Thus, these materials can be regarded as "molecules," if somewhat exotic ones.

On the other hand, there is another class of metal nanoparticles in solutions, which are stabilized by polymeric materials. These nanoparticles are classical in concept, but still extremely useful, particularly as catalysts.[7] The most characteristic aspect of this type of nanoparticles, compared with the monolayer protected ones, is that the protecting molecules adsorb on the surface of the nanoparticles through weak, non-covalent interactions (van der Waals and/or electrostatic). The stability of the nanoparticles is then ensured by both the multiple-point interactions and the steric bulkiness of the polymers. The absence of strong covalent bonding between the nanoparticle surfaces and the protecting molecules is beneficial for these particles to exhibit catalytic activities. There have been efforts toward obtaining "molecularly dispersed" nanoparticles of this class by use of large, well-defined molecules such as dendrimers.[8] These approaches have been successful in presenting new nanoparticles that exhibit interesting chemical and physical properties, whereas elucidation of their structures and dynamics at molecular levels is yet to be done.

In this article, we wish to report studies on gold nanoparticles stabilized with tripod thioether oligomers **1a–c** (hereafter abbreviated as "TTO"), and applications of molecular-dynamic (MD) simulations for these materials. Since thioethers are expected to adsorb on gold nanoparticles via non-covalent interactions,[9] these are classified as weakly protected metal nanoparticles. The dynamic behavior of TTO on the nanoparticles was examined by analyzing the trajectory of the MD simulations. Computational chemistry will thus provide a reasonable basis for design and development of new organic–nanoparticle composite materials.

Results

Synthesis of the Tripod Thioether Oligomers (TTO). Scheme 1 shows the synthesis of the tripod thioether oligomers **1a–c**. The synthetic scheme is straightforward; the key reaction is the formation of dibenzyl sulfide function via a two-step procedure: (i) benzyl bromide or mesylate was allowed to react with thioacetic acid in the presence of DBU (1,8-diazabicyclo[5.4.0]undec-7-ene, an organic base), (ii) the resulting benzyl thioacetate was treated with hydroxide in the presence of another benzyl halide. Similar procedures were utilized by Ono et al. for synthesis of oligo(dibenzyl sulfide)s as precursors of oligo(phenylene vinylene)s,[10] and more recently by Chow et al. for oligo(dibenzyl sulfide) dendrimers.[11]

Synthesis and Characterization of Gold Nanoparticles Stabilized with TTO. The gold nanoparticles stabilized by **1a–c** were prepared by the two-phase method[4] with slight modifications. The resulting deep brown solution was successively passed through a 0.2-μm syringe filter and an alumina column, followed by three repeated centrifugations of a turbid solution in CH_2Cl_2/EtOH at 10000 rpm for 5 min. The filtration and alumina chromatography removed the large or associated particles (monitored by disappearance of the plasmon resonance at 520 nm in the UV–vis absorption spectra) and unchanged tripod molecules (monitored by TLC); the centrifugation removed the phase-transfer reagent Oct_4NBr (monitored by ^{1}H NMR). The purified materials, expressed as **1a–Au**, **1b–Au**, and **1c–Au** hereafter, were deep brown waxy oils that were soluble in $CHCl_3$, THF, and toluene, and insoluble in MeOH, EtOH, and water. Both the chloroform solutions and the evaporated waxy materials can be kept in a freezer under Ar for several weeks without change. When the above procedure was carried out without addition of **1a–c**, only black precipitates and colorless supernatants formed. This suggests that

Published on the web October 4, 2005; DOI 10.1246/bcsj.78.1773

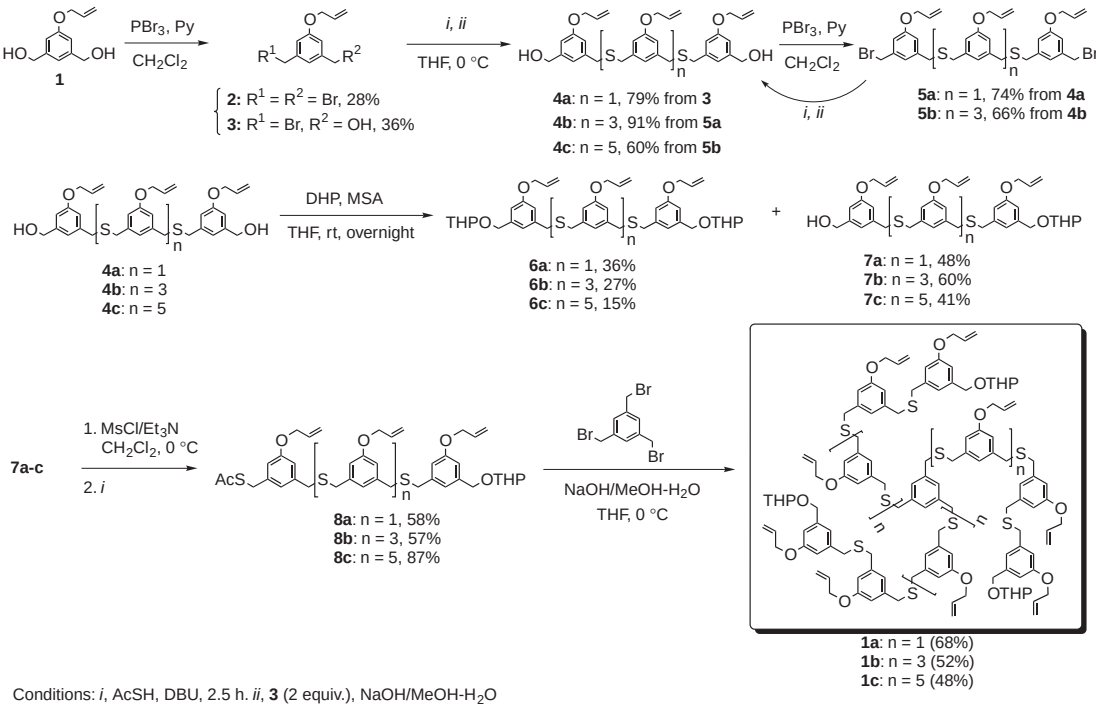

Scheme 1.

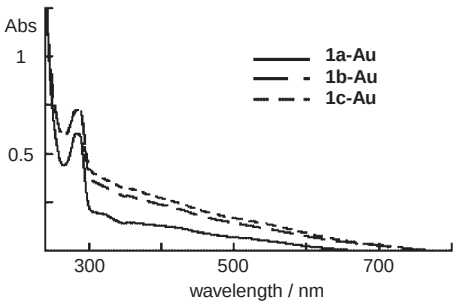

Fig. 1. UV–vis absorption spectra of **1a**–**Au**, **1b**–**Au**, and **1c**–**Au** in $CHCl_3$.

1a–**c** indeed worked as a stabilizer of gold nanoparticles. The ligands **1a**–**c** were slowly replaced with stronger ligands such as alkanethiols. When **1c**–**Au** (0.60 mg) was treated with 1-dodecanethiol (0.43 mg) in CH_2Cl_2 (1 mL) for 7 d, free **1c** and dodecanethiol-protected gold nanoparticle were detected by ^{1}H NMR, UV–vis, and TLC (silica gel, CH_2Cl_2/EtOAc), together with some unidentified decomposition products.

The UV–vis absorption spectra of the purified **1a**–**Au**, **1b**–**Au**, and **1c**–**Au** in $CHCl_3$ are shown in Fig. 1, revealing the absorbance of aromatic rings (280 nm) and gold nanoparticles (400–800 nm). The absence of characteristic plasmon resonances (520 nm) suggests that the particle sizes were less than 2 nm.[12] Figure 2 shows the TEM images of gold nanoparticles and the size-distribution histograms made by counting the particles, together with the plot of the size-distribution curves obtained from the SAXS analyses. The mean particle sizes estimated from the TEM images were 1.5–1.7 nm, with no particular trends with the sizes of the protecting molecules. The SAXS analyses gave somewhat smaller values, but the differences with the TEM results were well within the estimated standard deviations. These results suggest that the particle sizes are mainly controlled by the thermodynamics and/or kinetics of formation of the particles, rather than by the size and shape of the stabilizing molecules. Interestingly, the sizes of these nanoparticles were smaller than the sizes of other gold nanoparticles stabilized by thioethers[10] or other weakly binding stabilizers (1.8–6.5 nm),[13] and were close to the sizes of gold nanoparticles protected by straight-chain alkanethiols.[4] We attribute this preferential formation of small particles to the multiple-point interaction between **1a**–**c** and the nanoparticles.

The ICP-AES analyses of **1a**–**Au**, **1b**–**Au**, and **1c**–**Au** gave relative abundances of Au/S = 0.77, 0.54, and 0.63 (in number of atoms). On the other hand, the mean number of gold atoms in nanoparticles were 175 ± 130, 187 ± 170, and 126 ± 82 for **1a**–**Au**, **1b**–**Au**, and **1c**–**Au**, as estimated from the TEM images. From these values, the number of protecting molecules per nanoparticles were estimated as 25 ± 19, 23 ± 21, and 10 ± 6. Although molecular models suggest that **1a**–**c** are of comparable sizes with the sizes of nanoparticles observed by TEM, the observed number of protecting molecules per nanoparticle was much greater than unity. We will discuss later about a plausible model to account for these results.

Molecular Dynamics. In order to get insights about the structures of these composite materials, we carried out molecular-dynamic simulations. Our study consisted of three stages: (i) development of the parameters that describe the interaction between the gold nanoparticles and TTO, (ii) preliminary simulations of TTO alone, and (iii) simulations of the nanoparticle–TTO composite systems. For the sake of simplicity, we will hereafter limit our discussion to the smallest TTO molecule (**1a**).

Development of Gold–TTO Parameters. There are many studies on molecular-dynamic simulations of chemisorbed thiols on a gold surface,[14] and some studies on simulations

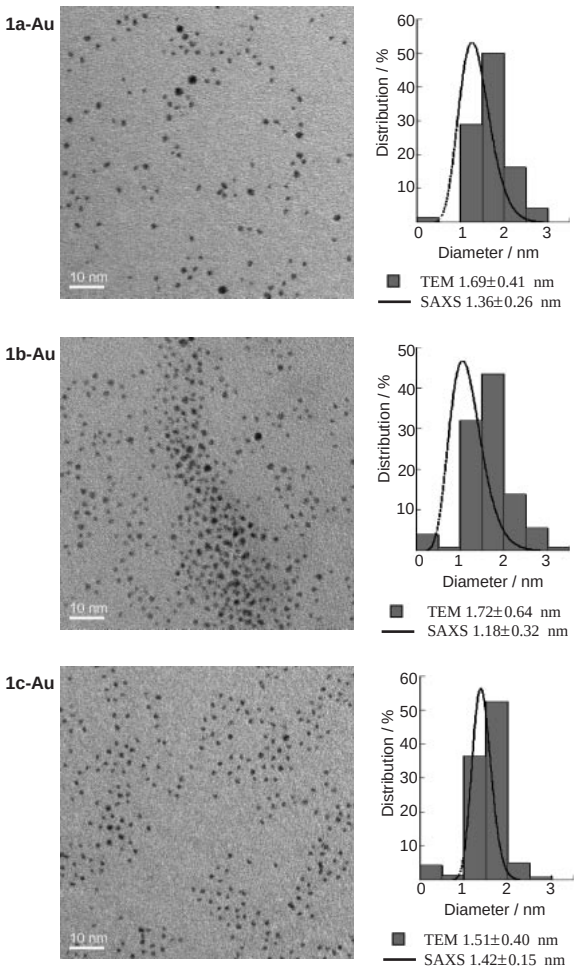

Fig. 2. TEM images and histograms with SAXS plots (in THF) of **1a–Au**, **1b–Au**, and **1c–Au**.

of naked gold nanoparticles,[15] but there are very few reports on simulations of composites of gold nanoparticles and organic molecules.[16] In particular, there are no reports on simulations of *physisorbed* organic molecules on gold nanoparticles. Therefore, we first need to develop reasonable parameters that can describe the interactions between the gold nanoparticles and physisorbed organic molecules.

Because the physisorption energies of organic molecules on gold nanoparticles have not been measured, we used the physisorption energies on the Au(111) surface as the basis of our parameter development. Lavrich and co-workers[17] measured the physisorption enthalpies of various sulfur-containing molecules on the Au(111) surface. Their results revealed that the physisorption enthalpies could be predicted as the sum of the following values (in kJ/mol) for each group which directly contacts with the surface: 15.5 (CH_3–), 6.1 (–CH_2–), 9.1 (sp^2–CH=), 33.5 (HS–), and 24.1 (–S–). This empirical formula implies that the adsorption energy is additive in regard to the number and kind of the surface-contacting non-hydrogen atoms. Thus we can reasonably assume that the adsorption potential energy is the sum of the atom–surface interaction potentials:

$$V_{\mathrm{ads}} = \sum_i V_i(\mathbf{r}_i), \tag{1}$$

Table 1. The Pair-Specific van der Waals Parameters for the Au(surface)–X Pairs

X	ε(X)/(kcal/mol)	r_0(X)/Å
C_{Me}	0.81	3.84
C_{CH_2}	0.32	3.84
C_{sp^2}	0.48	3.73
S_{SH}	1.75	3.56
S_{SR}	1.26	3.56

where i covers the indices of non-hydrogen atoms in the adsorbent molecule and $V_i(\mathbf{r}_i)$ is the atom–surface potential of the adsorbent atom i. Our next problem is to express $V_i(\mathbf{r}_i)$ as a realistic and computationally tractable function. Beardmore et al.,[18] in their MD simulations of alkanethiol monolayers on Au(111), fitted the potential as a Morse function of the distance between the adsorbent atom and the gold surface. This is a reasonable formulation, but in our case it is not applicable because the distance from the "surface of the nanoparticle" can not be defined unequivocally. Instead, we use a pair-specific van der Waals potential function between the adsorbent atom and the surface gold atom, and assume that $V_i(\mathbf{r}_i)$ can be expressed as the sum of the pair potentials over all the surface gold atoms. Then Eq. 1 becomes:

$$V_{\mathrm{ads}} = \sum_i \sum_j \varepsilon(\mathrm{X}_i)\left\{\left(\frac{r_0(\mathrm{X}_i)}{r_{ij}}\right)^{12} - 2\left(\frac{r_0(\mathrm{X}_i)}{r_{ij}}\right)^{6}\right\}, \tag{2}$$

where i and j are the indices of the adsorbent (non-hydrogen) atoms and the surface gold atoms, respectively, X_i is the atom type of the adsorbent atom i (which is one of C_{Me}, C_{CH_2}, C_{sp^2}, S_{SH}, and S_{SR}, corresponding to the five adsorbent atom types described above), and ε(X) and r_0(X) are the pair-specific van der Waals parameters which depend on the adsorbent atom types. The values of ε(X) and r_0(X) were optimized so that the calculated adsorption energies of selected molecules matched the experimental enthalpies (see: Computational Methods for details). The obtained values are shown in Table 1.

Simulations of TTO. Prior to the simulations of the nanoparticle–TTO systems, we examined the molecular-dynamic simulations of TTO alone. The purpose of this preliminary study was to examine the effect of the solvent on the conformation of TTO. Thus, we compared two independent simulations of **1a**, one without solvent and the other with explicit $CHCl_3$ solvent, starting from the same, arbitrary initial conformation. Figure 3 shows the changes of the distances between the center of the central benzene ring and the three acetal carbons of the THP groups. These distances conveniently indicate the conformations of the three legs of the tripod molecule. Without solvent (part (a)), all the legs quickly collapsed to folded conformations (distances less than $<$15 Å) and never got unfolded again, because of strong intramolecular van der Waals attractive interactions. On the other hand, with solvent (part (b)) each leg went back and forth between the folded and extended conformations during 4×10^6 MD steps (=8 ns). Collapse was avoided because intramolecular van der Waals interaction was compensated by the solvation energy. These results suggest that the solvent must be included in the MD simulation of these systems. We carried out all the following simulations with explicit solvents.

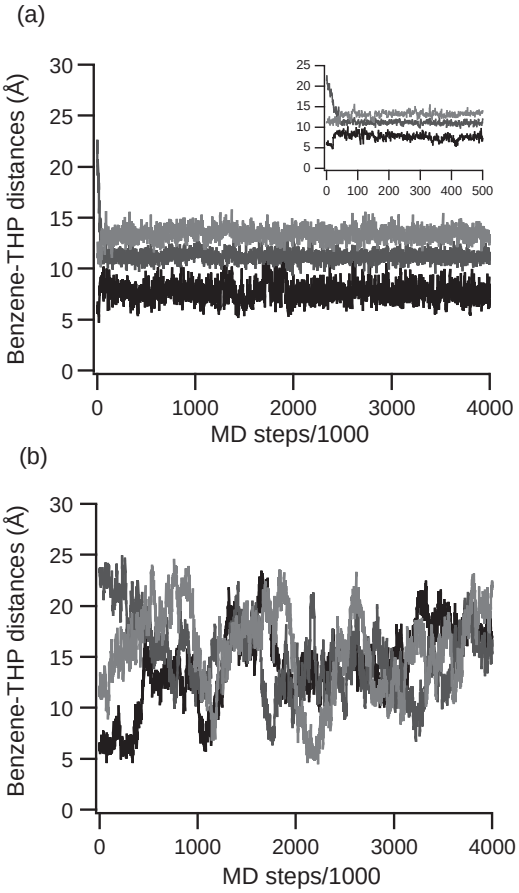

Fig. 3. Distances between the center of the central benzene ring and the acetal carbons of the THP groups in the MD trajectory at 300 K. (a) **1a** in a vacuum, (b) **1a** with explicit $CHCl_3$ solvent. The three traces correspond to the three "legs" of **1a**.

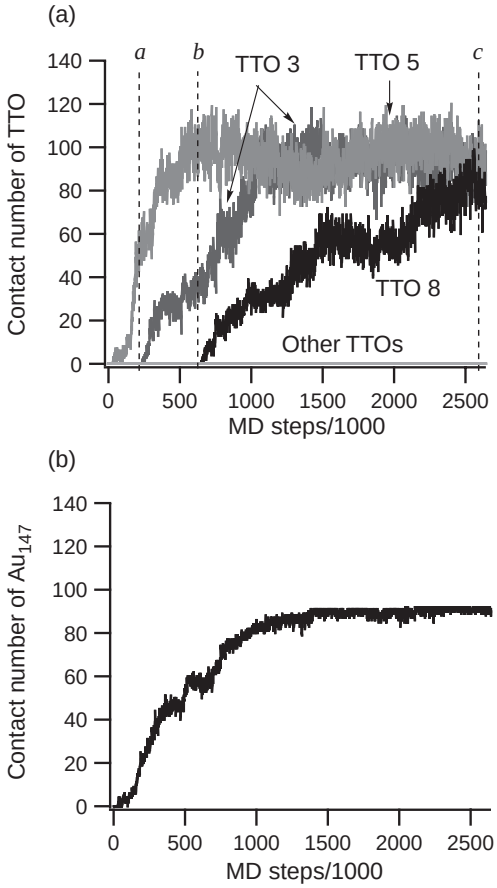

Fig. 4. The contact numbers of (a) **1a** molecules and (b) the gold nanoparticle in the simulation of 16 **1a** and Au_{147} with explicit $CHCl_3$ solvent. The vertical lines noted *a*, *b*, and *c* in part (a) correspond to the snapshots shown in Fig. 5.

Simulations of Gold Nanoparticle–TTO Systems. Simulation of gold nanoparticle–TTO systems were carried out by placing TTO molecules around a naked gold nanoparticle and subjecting the whole system to MD runs with explicit $CHCl_3$ solvent at 300 K. Although this does not reproduce the real process under the experimental conditions (which includes simultaneous growth of gold nanoparticles and adsorption of TTOs), it will give us useful information about the possible structures of the resulting composites of gold nanoparticles and TTOs. A cuboctahedron Au_{147} (diameter 1.7 nm) was used as a model of the gold nanoparticle.

Figure 4 shows the results from a single run, in which 16 TTO molecules (**1a**) and an Au_{147} nanoparticle were placed in a box of $CHCl_3$ with dimensions $112.2 \times 96.3 \times 97.7$ Å^3. Part (a) shows the plots of "contact numbers" of the individual TTO molecules versus the MD steps, where the contact number of a TTO molecule is defined by the number of atoms of the TTO molecule that are within 3.84 Å of any surface atom in the gold nanoparticle (the choice of 3.84 Å as the cutoff value is based on the pair-specific van der Waals parameters in Table 1). Part (b) shows the contact number of the gold nanoparticle, which is defined by the number of the surface gold atoms that are within 3.84 Å of any atom in any TTO molecule. From part (a), we see that 3 TTO molecules are adsorbed to the gold nanoparticle. As more atoms in the TTO molecules get adsorbed, the contact number of the gold nanoparticle (part (b)) monotonically increases to 88–92, which means that more than 95% of the nanoparticle surface is covered with TTOs (the number of surface atoms in Au_{147} is 92). We performed two more runs under similar conditions with different starting locations and orientations of the TTO molecules; the numbers of adsorbed TTO molecules were 3 and 4, and the final contact numbers of gold nanoparticles were 85–87 and 90–92. These results indicate that 3–4 molecules of TTO (**1a**) are sufficient to cover the entire surface of an Au_{147} nanoparticle.

Figure 5 illustrates how the TTO molecules are adsorbed on the surface of a gold nanoparticle. Three representative snapshots were selected so that one, two, and three TTO molecules were adsorbed (later we will discuss the 1:1 complexes in more detail). It is easily seen that the surface is completely covered with three TTO molecules in this case. Figure 5 also illustrates the distribution of contacting atoms in each adsorbing TTO molecule, indicating the multiple-point interaction between the gold nanoparticle and TTOs. It should also be noted that not only the sulfur atoms but also the carbon atoms (both aromatic and benzylic) participate in adsorption. This is reasonable because the pair-specific van der Waals parameters

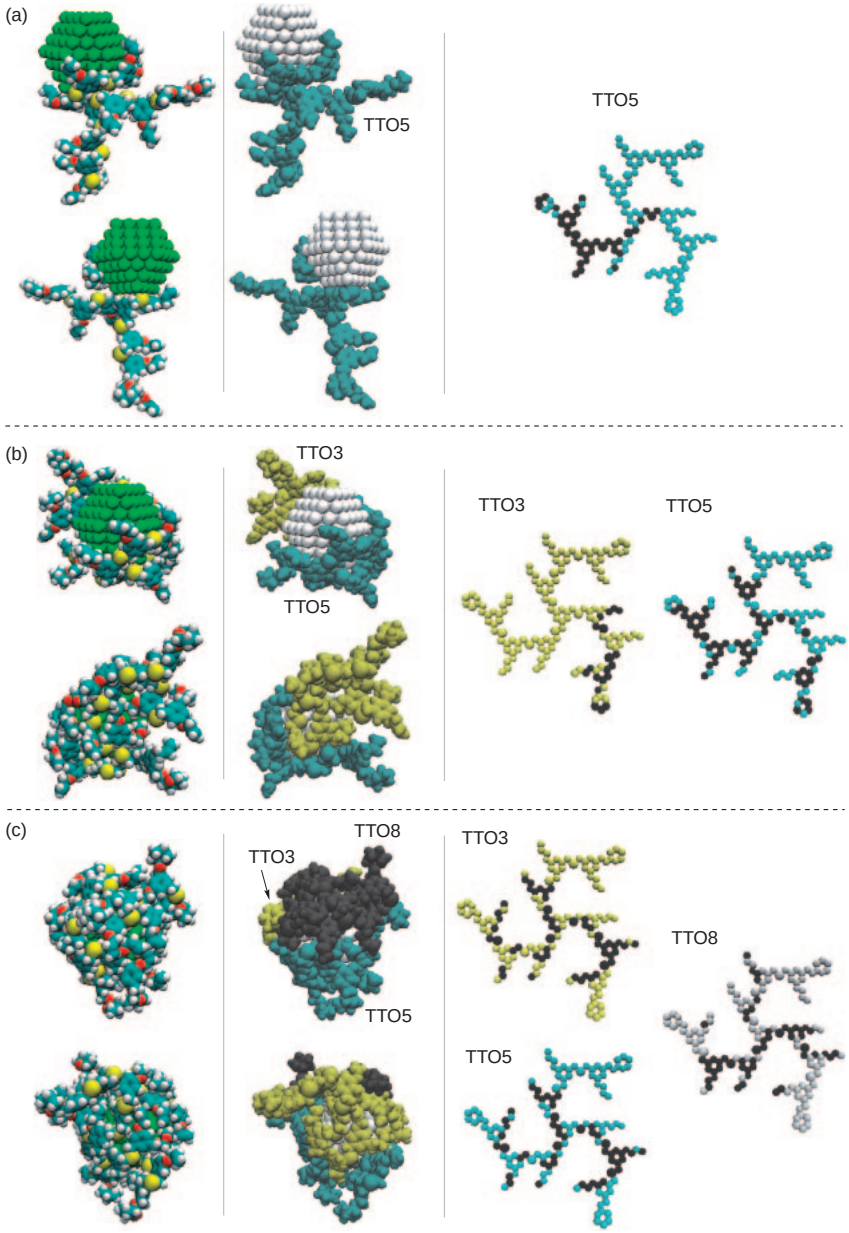

Fig. 5. Three selected snapshot structures from the $\mathbf{1a}_{16}/Au_{147}$ simulation shown in Fig. 4. Left column: the space-filling views from two opposite directions (green: gold, cyan: carbon, white: hydrogen, red: oxygen, and yellow: sulfur). Middle column: the space-filling views with different colors for different molecular fragments; the gold nanoparticle is shown in white, and the TTO (**1a**) molecules are shown in blue, yellow, and gray. Right column: the contacting atoms in each **1a** molecule (black circles). Parts (a), (b), and (c) correspond to the vertical lines shown in Fig. 4a.

in Table 1 indicate that both aliphatic and aromatic carbon atoms have significant interaction energies (25–65% of that of thioether sulfur atom).

The next question we would like to answer is this: how many surface gold atoms can a *single* TTO molecule cover? The results in the above paragraph suggest an average number of $92/3 \approx 31$, but this is the number when multiple TTO molecules are bound simultaneously. To examine the coverage by a single TTO molecule, we performed simulations of a 1:1 complex of Au_{147} and **1a**. Figure 6 shows the results from three independent runs with different starting orientations. The final contact numbers of Au_{147} range from 40 to 65. This corresponds to 45–70% coverage. Part (c) of Fig. 6 also shows the van der Waals interaction energies (not including the solvents) at each MD step. As expected, the van der Waals energies decrease with increasing contact numbers due to the attractive force between **1a** and Au_{147}. Figure 7 illustrates how each single **1a** covers the surface of Au_{147}, by showing the conformations of the Au_{147}–**1a** composites and the contacting atoms in the **1a** molecule at the timesteps which gave the largest (i.e. the most negative) van der Waals interaction energies for each run. Table 2 compiles the timesteps, interaction energies, and the contact numbers of **1a** and Au_{147} for the snapshots shown in Fig. 7. The conformations from Runs 1 and 3 show that all three legs of the tripod molecule **1a** bind to the Au_{147} surface via multiple-point interactions, whereas

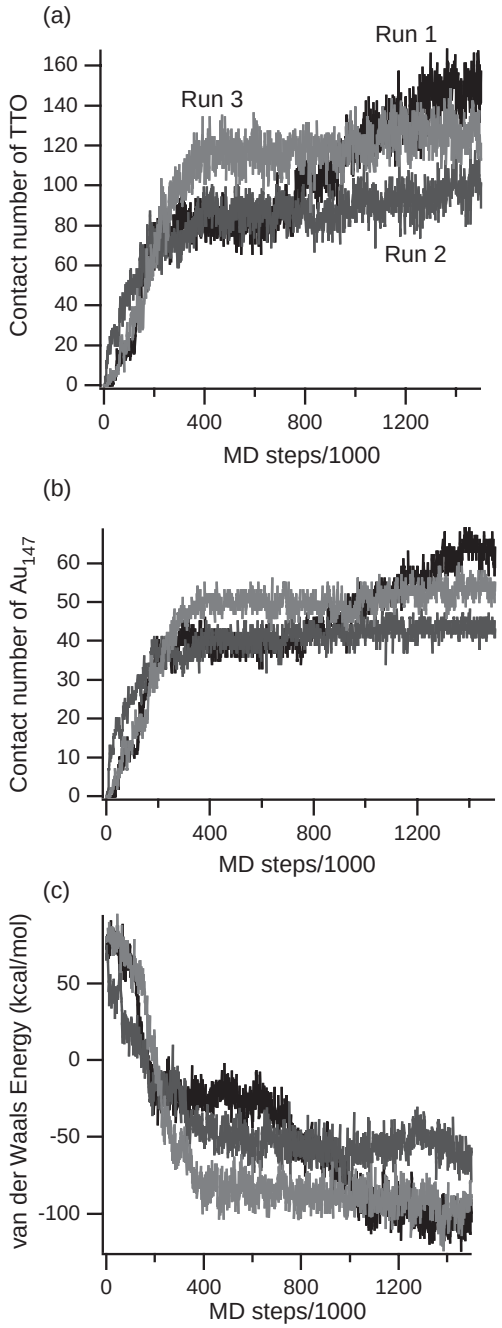

Fig. 6. The contact numbers of (a) **1a** and (b) Au_{147}, and (c) the interaction energy between **1a** and Au_{147}, in the three independent simulations of 1:1 **1a** and Au_{147} with explicit $CHCl_3$ solvent.

the conformation from Run 2 shows that one of the legs remains almost unbound. It is likely that Run 2 would have given a similar result with Runs 1 and 3 if the simulation was performed for a longer period; actually, Figures 6a and 6b indicate that Run 1 was temporary trapped in a similar conformation as the final state of Run 2 during $4–6 \times 10^5$ MD steps, and then "escaped" to the more stable conformations. This type of "trapping" phenomena, which is caused by the presence of many local minima in the potential energy surface, is a well-known problem in simulations of large molecules.[19]

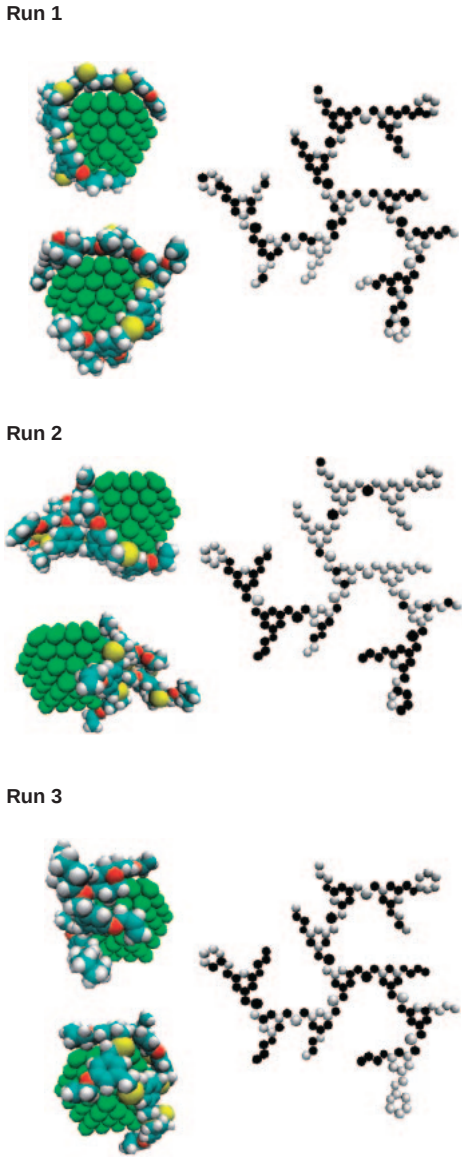

Fig. 7. The structures of lowest interaction energies in the three independent simulations of 1:1 **1a** and Au_{147}. The left column shows the space-filling views from two opposite directions (green: gold, cyan: carbon, white: hydrogen, red: oxygen, and yellow: sulfur) and the right column shows the contacting atoms in **1a** (black circles).

Table 2. The Energies and Contact Numbers at the Maximum Interaction Steps[a] in **1a**/Au_{147}

Run	MD step /1000	Interaction energies[b] /kcal mol^{-1}	Contact numbers	
			1a	Au_{147}
1	1457	−124.2	149	64
2	971	−82.4	96	46
3	1386	−123.8	129	54

a) The "maximum interaction step" is defined as the MD step in which the van der Waals interaction energy of the **1a**/Au_{147} complex is the lowest. b) The van der Waals interaction energies of the **1a**/Au_{147} complex (not including the solvent).

There are various techniques to address this problem, and applications of these techniques to the present system are currently under way.

Discussion

The MD simulations showed that 3–4 molecules of **1a** were sufficient to cover the surface of a 1.7-nm gold nanoparticle, whereas the experiments showed as many as 25 molecules of **1a** were present per one gold nanoparticle. Although it is not impossible to accommodate more than 20 **1a**'s around the surface of a gold nanoparticle, the more appropriate model would be coexistence of free, unbound **1a** molecules and gold nanoparticles covered with a small number of **1a**. The free and bound **1a** molecules should be in dynamic equilibrium in $CHCl_3$ solutions, as indicated by the following observations: (i) the ^{1}H NMR spectra only showed one set of slightly broadened signals which were characteristic of nanoparticle-bound molecules and (ii) the gel permeation chromatography of **1a**–**Au** showed a complex feature with many peaks, and when a fraction corresponding to one peak was separated and injected again to the same GPC apparatus, a similar complex chromatogram was obtained again.

The sizes of TTOs are comparable to those of gold nanoparticles, if a little too small in the case of **1a**. Hence, in principle it is possible to design the TTO to form 1:1 complexes with gold nanoparticles, like in the beautiful work by Inomata and Konishi.[20] However, in the present study, the molecular design of TTOs was too crude to realize such well-defined composites. De Cola et al.[21] reported gold nanoparticles by use of a series of oligo(thioether) dendritic compounds with a similar aim, but even their extensive study did not lead to conclusive evidence for 1:1 complexes. On the other hand, works of Watanabe[22] and Aida[23] introduced a concept of well-defined composites of nanoparticles and proteins with predetermined hollows. The use of proteins is beneficial in that they have well-defined structures and are even controllable by use of biological functions, but such use has the drawback that their designs are determined by nature and modification of their functions is limited. Admittedly, the apparent problem in designing the artificial molecules from scratch to form well-defined complexes with nanoparticles is the great conformational flexibility that makes prediction of the structure too difficult. The lack of experimental methods to examine the solution structure is also problematic.

Molecular dynamic simulations can be a powerful tool to overcome these difficulties. Although the MD methods also have their specific technical problems (among them is the "trapping in the local minima" problem mentioned earlier), they have already been used extensively for studying dynamics of large molecules in solutions, including proteins. The present article demonstrates the applicability of MD to the gold nanoparticles stabilized with thioether organic molecules, and our ongoing studies will unveil more power of these methods in development of new soft nanomaterials.

Experimental

General. Tetrahydrofuran (THF) and diethyl ether were distilled from sodium diphenylketyl. Dichloromethane was distilled from calcium hydride. Other chemicals were used as received. ^{1}H and ^{13}C NMR spectra were recorded on JEOL Lambda 500. Melting point were determined by Yanaco MP-500V (uncorrected values). UV–vis spectra were measured by Shimadzu UV-2500PC. Transmission electron microscopy (TEM) images were recorded by the JEOL JEM-2000EX. Medium-pressure column chromatography was carried out by use of Wakogel C-200 or neutral alumina Merck Art. 1097 Aluminiumoxid 90. Analytical thin layer chromatography (TLC) was performed on Merck TLC aluminum sheets (silica gel RP-18 F_{254} and aluminum oxide 60 F_{254}). Preparative gel permeation chromatography (GPC) was carried out on LC-908 (Japan Analytical Industry Co.) equipped with the polystyrene-based columns JAIGEL-2.5H and 2H ($CHCl_3$, 3.5 mL/min). Small-angle X-ray scattering was measured on a Rigaku ATX diffractometer. The average diameter and variance were obtained by assuming the Γ-distribution function for the size distribution of the nanoparticles and fitting the observed scattering intensities to the analytical expression.[24]

Synthetic Procedures. Only general procedures are described in the following. The amounts of reagents for the individual steps and the compound data for characterization can be found in the Supporting Information.

Bromination with PBr_3. A solution of the diol in pyridine/CH_2Cl_2 was placed in a round-bottomed flask with a magnetic stirring bar and a three-way stopcock. Phosphorus tribromide was slowly added at 0 °C and the reaction mixture was stirred under argon at rt. After 24 h, the reaction mixture was quenched with water and extracted with CH_2Cl_2. The organic phase was dried over anhydrous $MgSO_4$. The solvent was evaporated, and the residue was purified by medium-pressure column chromatography (CH_2Cl_2).

Thioacetylation (Step (i)). A mixture of the bromide (or mesylate), thioacetic acid, and THF was placed in a two-necked flask with a magnetic stirring bar, a three-way stopcock, and a pressure-equalizing dropping funnel protected with a rubber septum. A THF solution of DBU was dropped slowly at 0 °C under argon, and the reaction mixture was stirred at rt. After 5 h, the reaction mixture was quenched with water and extracted with hexane. The organic phase was dried over anhydrous $MgSO_4$. The solvent was evaporated to give the desired thioacetate as a yellow oil, which was used in the next reaction without further purification.

Preparation of Dibenzyl Sulfides (Step (ii)). A solution of the thioacetate and the bromide in THF was placed in a round-bottomed flask with a magnetic stirring bar and a pressure-equalizing dropping funnel equipped with a three-way stopcock. Argon gas was bubbled through the solution for 30 min. A solution of NaOH in MeOH/H_2O (v/v = 4/1) was added dropwise under argon at 0 °C, and the solution was stirred overnight at rt. The reaction mixture was quenched with water and extracted with CH_2Cl_2. The organic phase was dried over anhydrous $MgSO_4$. The solvent was evaporated, and the residue was purified by medium-pressure column chromatography (hexane/EtOAc).

Monoprotection of Diols by THP. A solution of the diol and 3,4-dihydro-2*H*-pyran in THF was placed in a round-bottomed flask with a magnetic stirring bar and a three-way stopcock with a rubber septum. Methanesulfonic acid was added at rt under argon, and the reaction mixture was stirred overnight at rt. The reaction mixture was quenched with water and extracted with CH_2Cl_2. The organic phase was dried over anhydrous $MgSO_4$. The solvent was evaporated, and the diol, the mono-THP ether, and the di-THP ether were separated by medium-pressure column chromatography (hexane/EtOAc). The di-THP ether was

converted back to the diol for recycle by treatment with *p*-toluenesulfonic acid (0.25 equiv per THP group) in CH_2Cl_2/MeOH (v/v = 2/1, rt, overnight).

Preparation of Mesylates. A mixture of the alcohol, methanesulfonyl chloride, and CH_2Cl_2 was placed in a round-bottomed flask with a magnetic stirring bar and a three-way stopcock. Triethylamine was added at 0 °C under argon atmosphere, and the reaction mixture was stirred for 2–4 h. The reaction mixture was quenched with water and extracted with CH_2Cl_2. The organic phase was dried over anhydrous $MgSO_4$. The solvent was evaporated to give the corresponding mesylate as colorless oil, which was used in the next reaction without further purification.

Preparation of Gold Nanoparticles Stabilized with TTO. An aqueous solution of $HAuCl_4$ (2.25 mM, 1 mL) was combined with a $CHCl_3$ solution (1 mL) of Oct_4NBr (2.25 μmol) and the tripod molecules **1a–c** (**1a**: 0.55 mg, 0.25 μmol; **1b**: 0.50 mg, 0.15 μmol; **1c**: 0.48 mg, 0.11 μmol). The two-phase mixture was vigorously stirred (ca. 1500 rpm) for 10 min at rt until the aqueous layer turned to colorless and the organic layer turned to yellow. To this mixture, a freshly prepared aqueous solution of $NaBH_4$ (75 mM, 30 μL) was added with vigorous stirring. After 10 min, the color of organic layer changed to deep brown. The organic layer was filtered through a 0.2-μm syringe filter and then purified by alumina column chromatography eluting with 4:1 dichloromethane–methanol, followed by three repeated centrifugations of a turbid solution in CH_2Cl_2/EtOH at 10000 rpm for 5 min.

Computational Methods

General. The initial geometries of the organic molecules were obtained by building the molecular model with the Chem3D program package (CambridgeSoft). The structure and coordinate files of appropriate format were generated by a homemade program suite named PSFLIB. The atom types and force field parameters were taken from the parm99 force field distributed with AMBER 7.[25] The RESP (restrained electrostatic potential fit) atomic charge[26] were obtained by quantum mechanical calculation (HF/6-31G*) with GAMESS,[27] followed by treatment with the RESP module of AMBER with the aid of the R.E.D. script.[28] The molecular dynamics calculation was performed with NAMD package.[29] A timestep of 2 fs was used. The temperature was maintained by reassigning the velocities every 500 steps. The RATTLE constraint[30] was applied to all hydrogen atoms. A 10-Å cutoff was applied to non-bonding interactions. Simulation with explicit solvents was performed under periodic boundary conditions with a constant volume, and the long-range electrostatic forces were evaluated by the particle mesh Ewald method.[31] The trajectory was analyzed with VMD[32] and homemade programs. Calculations were performed on a Silicon Graphics SGI2800 computer of Research Center of Computational Science (Okazaki Research Facilities, National Institutes of Natural Sciences) and a local cluster of Apple PowerMac G5 machines.

Development of Gold–TTO Parameters. The following molecules were used to determine the gold–TTO parameters: CH_3SH, CH_3CH_2SH, $CH_3(CH_2)_3SH$, $CH_3(CH_2)_5SH$, $CH_3(CH_2)_7SH$, $CH_3(CH_2)_8SH$, $(C_2H_5)_2S$, $(C_4H_9)_2S$, and thiophene. The experimental values of physisorption enthalpies (ΔH_{expt}) of these molecules on Au(111) were taken from Ref. 17. On the other hand, the "calculated" physisorption enthalpies were obtained in the following way: (i) a planar hexagonal array of 169 gold atoms with the interatomic distance of 2.88 Å was prepared, (ii) the target molecule (one of the above nine) was placed along the plane 4.0 Å above the gold plane, (iii) the total energy of the system (E_0) was calculated with the surface interaction potential (Eq. 2) switched off, (iv) the surface interaction potential was switched on and the system was subjected to molecular dynamic simulation at 300 K for 2 fs × 10000 steps, then to the energy minimization (E_1), and (v) the calculated physisorption enthalpy ΔH_{calc} was obtained as $E_1 - E_0$.

Optimization of $\varepsilon(X)$ and $r_0(X)$ was carried out as follows. Since only 9 experimental values were available to determine 10 parameters, all parameters cannot be optimized independently. Instead, four coefficients (K_1, K_2, K_3, and K_4) were introduced and $\varepsilon(X)$ and $r_0(X)$ were expressed as follows:

$$\varepsilon(X) = K_1 \cdot A(X), \tag{3}$$

$$r_0(X) = K_n \cdot (r_{vdW}(X) + r_{vdW}(Au)) \quad (n = 2 \text{ for } X = C_{Me} \text{ and } C_{CH_2},\ n = 3 \text{ for } X = C_{sp^2},\ n = 4 \text{ for } X = S_{SH} \text{ and } S_{SR}), \tag{4}$$

where $A(X)$ is the empirical adsorption energy per group consisting of an atom X and attached hydrogens (Ref. 17; the values are also quoted in the text), and $r_{vdW}(X)$ is the van der Waals radius of atom X. The following iterative algorithm was employed to find the optimized set of coefficients K_1–K_4:

(1) Initial guess values of $K_1 = 0.22$, $K_2 = K_3 = K_4 = 1.0$ and a "scaling factor" $k = 0.01$ are set.

(2) The ΔH_{calc} of the nine model molecules and the squared sum of residuals $R = \Sigma(\Delta H_{calc} - \Delta H_{expt})^2$ are calculated. The initial value of R is kept as R_{ini}.

(3) A trial move is attempted by the amount $\Delta K_i = (\text{Ranf} - 0.5) \cdot kR/R_{ini}$, where Ranf is a uniform random number in [0, 1] (different Ranf for different i).

(4) For the new set of $K_i' = K_i + \Delta K_i$, ΔH_{calc} and R are calculated.

(5) If R is smaller than the previous value, then this trial is accepted and K_i valus are updated. Return to (4) with the same trial move ΔK_i.

(6) If R is larger than the previous value, then this trial is rejected and K_i are unchanged. Return to (3) to try different direction.

(7) If the probability of rejection becomes too high (>0.8), then k is reduced (multiplied by 0.25). If k is sufficiently small, then the local minimum is achieved and the calculation ends.

The final R was 3.10 $kcal^2/mol^2$, and the maximum/minimum of residuals were +0.97 and −1.28 (in kcal/mol), respectively.

Simulations of TTO. To calculate the RESP charges efficiently, we divided the target molecule **1a** into ten fragments so that each fragment contained one benzene ring, and the charges were calculated for each fragment plus appropriate capping groups. The structure of each fragment and the resulting RESP charges can be found in the Supporting Information. After the charges were assigned to all atoms in **1a**, a rectangular box of $CHCl_3$ was added providing at least 10 Å of $CHCl_3$ around any solute atom. The atomic coordinates and

parameters for $CHCl_3$ were taken from Caldwell's work.[33] The system was subjected to energy minimization for 1000 steps, gradual heating from 0 to 300 K over 15000 steps, preequilibration at 300 K for 250000 steps, and production run at 300 K for 4000000 steps. For the vacuum simulation, a snapshot was taken from the solvated simulation after the preequilibration, all the solvent molecules were removed, and the resulting naked **1a** was subjected to production run at 300 K (without periodic boundary conditions) for 4000000 steps.

Simulations of Gold/TTO Systems. A set of atomic coordinates for an ideal cuboctahedral Au_{147} was created with the Au–Au distances of 2.88 Å (= the interatomic distance in metallic gold). In the present study, the conformational change of the gold nanoparticle is not taken into account; hence, Au–Au bonds with equilibrium length 2.88 Å and force constant 200 kcal/mol/Å were assumed between all neighboring gold atoms. Bond angles and dihedrals were not included. Different atom types were assigned for the surface and internal gold atoms, so that the pair-specific van der Waals potentials (see: text for details) between the gold atoms and the TTO atoms should work only for the surface gold atoms. Ninety-two gold atoms out of 147 were assigned as the surface atoms.

The starting structures of the simulation of 16 TTOs and Au_{147} were generated in the following protocol: (i) the Au_{147} was placed at (0, 0, 0), (ii) 16 points were generated by use of the Halton sequence of quasi-random points[34] within a cube of 78-Å edges centered at (0, 0, 0), (iii) for each of the 16 points, a random conformation was selected from the trajectory of the simulation of solvated **1a** and placed at the point, and the placed molecule was rotated by random angle until no atom collisions were found, and (iv) if the molecule could not placed in any orientation, this point was discarded and another point was generated. The mean intermolecular distance was about 40 Å. To the resulting set of molecules, a rectangular box of $CHCl_3$ was added, providing at least 4 Å of $CHCl_3$ around any solute atom, and the system was subjected to the following sequence of simulations: (i) energy minimization for 1000 steps, (ii) gradually heating from 0 to 300 K over 15000 steps, and (iii) production run at 300 K for 3000000 steps. The simulation of 1:1 complexes of TTO and Au_{147} was carried out in a similar manner, except that only one TTO was placed around the gold nanoparticle.

We thank Dr. Osamu Oishi (IMS) for TEM measurement, Mr. Akito Sasaki (Rigaku Co.) for SAXS measurement and analysis, and the Research Center for Computational Science of Okazaki Research Facilities, National Institutes of Natural Sciences (NINS) for the use of the SGI2800 computer. This work was supported by a Grant-in-Aid for Scientific Research in Priority Area, "Reaction Control of Dynamic Complexes" (No. 16033262) and "Nanotechnology Support Project" of the Ministry of Education, Culture, Sports, Science and Technology (MEXT), Japan.

Supporting Information

Details of synthetic procedures and compound data (6 pages), and the details of RESP charge calculations (1 page). This material is available free of charge on the web at http://www.csj.jp/journals/bcsj/.

References

1 a) D. L. Feldheim, C. A. Foss, Jr., and M. Dekker, "Metal Nanoparticles," New York (2002). b) M.-C. Daniel and D. Astruc, *Chem. Rev.*, **104**, 293 (2004).

2 J. J. Pietron, J. F. Hicks, and R. W. Murray, *J. Am. Chem. Soc.*, **121**, 5565 (1999).

3 P. Claus, A. Brueckner, C. Mohr, and H. Hofmeister, *J. Am. Chem. Soc.*, **122**, 11430 (2000).

4 M. Brust, M. Walker, D. Bethell, D. J. Schiffrin, and R. Whyman, *Chem. Commun.*, **1994**, 801.

5 A. C. Templeton, W. P. Wuelfing, and R. W. Murray, *Acc. Chem. Res.*, **33**, 27 (2000).

6 J. G. Worden, A. W. Schaffer, and Q. Huo, *Chem. Commun.*, **2004**, 518.

7 a) A. B. R. Mayer and J. E. Mark, *ACS Symp. Ser.*, **622**, 137 (1996). b) N. Toshima, *NATO ASI Ser., Ser. 3*, **12**, 371 (1996).

8 R. M. Crooks, M. Zhao, L. Sun, V. Chechik, and L. K. Young, *Acc. Chem. Res.*, **34**, 181 (2001).

9 a) X.-M. Li, M. R. de Jong, K. Inoue, S. Shinkai, J. Huskens, and D. N. Reinhoudt, *J. Mater. Chem.*, **11**, 1919 (2001). b) E. J. Shelley, D. Ryan, S. R. Johnson, M. Couillard, D. Fitzmaurice, P. D. Nellist, Y. Chen, R. E. Palmer, and J. A. Preece, *Langmuir*, **18**, 1791 (2002).

10 N. Ono, H. Tomita, and K. Maruyama, *J. Chem. Soc., Perkin Trans. 1*, **1992**, 2453.

11 H.-F. Chow, M.-K. Ng, C.-W. Leung, and G.-X. Wang, *J. Am. Chem. Soc.*, **126**, 12907 (2004).

12 a) M. M. Alvarez, J. T. Khoury, T. G. Schaaff, M. N. Shafigullin, I. Vezmar, and R. L. Whetten, *J. Phys. Chem. B*, **101**, 3706 (1997). b) T. G. Schaaff, M. N. Shafigullin, J. T. Khoury, I. Vezmar, R. L. Whetten, W. G. Cullen, P. N. First, C. Gutiérrez-Wing, J. Ascensio, and M. J. Jose-Yacamán, *J. Phys. Chem. B*, **101**, 7885 (1997).

13 a) S. Chen and R. W. Murray, *Langmuir*, **15**, 682 (1999). b) R. Wang, J. Yang, Z. Zheng, M. D. Carducci, J. Jiao, and S. Seraphin, *Angew. Chem., Int. Ed.*, **40**, 549 (2001). c) M.-K. Kim, Y.-M. Jeon, W. S. Jeon, H.-J. Kim, S. G. Hong, C. G. Park, and K. Kim, *Chem. Commun.*, **2001**, 667. d) Y. Zhou, H. Itoh, T. Uemura, K. Naka, and Y. Chujo, *Langmuir*, **18**, 277 (2002).

14 a) B. Park, M. Chandross, M. J. Stevens, and G. S. Grest, *Langmuir*, **19**, 9239 (2003). b) Y. Morikawa, T. Hayashi, C. C. Liew, and H. Nozoye, *Hyomen Kagaku*, **23**, 423 (2002). c) M. Tarek, K. Tu, M. L. Klein, and D. J. Tobias, *Biophys. J.*, **77**, 964 (1999). d) H. H. Jung, Y. D. Won, S. Shin, and K. Kim, *Langmuir*, **15**, 1147 (1999). e) T.-W. Li, I. Chao, and Y.-T. Tao, *J. Phys. Chem. B*, **102**, 2935 (1998). f) T. Bonner and A. Baratoff, *Surf. Sci.*, **377–379**, 1082 (1997). g) Z. Zhang, T. L. Beck, J. T. Young, and F. J. Boerio, *Langmuir*, **12**, 1227 (1996). h) J. Hautman and M. L. Klein, *J. Chem. Phys.*, **91**, 4994 (1989).

15 a) T. X. Li, S. M. Lee, S. J. Han, and G. H. Wang, *Phys. Lett. A*, **300**, 86 (2002). b) H.-S. Nam, N. M. Hwang, B. D. Yu, and J.-K. Yoon, *Phys. Rev. Lett.*, **89**, 275502 (2002).

16 a) K. L. Yin, Q. Xia, H. T. Xi, D. J. Xu, X. Q. Sun, and C. L. Chen, *THEOCHEM*, **674**, 159 (2004). b) B. Arezki, A. Delcorte, A. C. Chami, B. J. Garrison, and P. Bertrand, *Nucl. Instrum. Methods Phys. Res., Sect. B*, **212**, 369 (2003).

17 D. J. Lavrich, S. M. Wetterer, S. L. Bernasek, and G. Scoles, *J. Phys. Chem. B*, **102**, 3456 (1998).

18 K. M. Beardmore, J. D. Kress, N. Grønbech-Jensen, and A. R. Bishop, *Chem. Phys. Lett.*, **286**, 40 (1998).

19 a) U. H. E. Hansmann and Y. Okamoto, *J. Comput. Chem.*,

18, 920 (1997). b) A. F. Voter, F. Montalent, and T. C. Germann, *Annu. Rev. Mater. Res.*, **32**, 321 (2002).

20 T. Inomata and K. Konishi, *Chem. Commun.*, **2003**, 1282.

21 A. D'Aleo, R. M. Williams, F. Osswald, P. Edamana, U. Hahn, J. van Heyst, F. D. Tichelaar, F. Vögtle, and L. De Cola, *Adv. Funct. Mater.*, **14**, 1167 (2004).

22 T. Ueno, M. Suzuki, T. Goto, T. Matsumoto, K. Nagayama, and Y. Watanabe, *Angew. Chem., Int. Ed.*, **43**, 2527 (2004).

23 D. Ishii, K. Kinbara, Y. Ishida, N. Ishii, M. Okochi, M. Yohda, and T. Aida, *Nature (London)*, **423**, 628 (2003).

24 a) K. Omote, Y. Ito, and S. Kawamura, *Appl. Phys. Lett.*, **82**, 544 (2003). b) O. Nagao, G. Harada, T. Sugawara, A. Sasaki, and Y. Ito, *J. Appl. Phys.*, **43**, 7742 (2004).

25 D. A. Case, D. A. Pearlman, J. W. Caldwell, T. E. Cheatham, III, J. Wang, W. S. Ross, C. L. Simmerling, T. A. Darden, K. M. Merz, R. V. Stanton, A. L. Cheng, J. J. Vincent, M. Crowley, V. Tsui, H. Gohlke, R. J. Radmer, Y. Duan, J. Pitera, I. Massova, G. L. Seibel, U. C. Singh, P. K. Weiner, and P. A. Kollman, Amber 7, University of California, San Francisco (2002).

26 C. I. Bayly, P. Cieplak, W. D. Cornell, and P. A. Kollman, *J. Phys. Chem.*, **97**, 10269 (1993).

27 M. W. Schmidt, K. K. Baldridge, J. A. Boatz, S. T. Elbert, M. S. Gordon, J. H. Jensen, S. Koseki, N. Matsunaga, K. A. Nguyen, S. J. Su, T. L. Windus, M. Dupuis, and J. A. Montgomery, *J. Comput. Chem.*, **14**, 1347 (1993).

28 A. Pigache, P. Cieplak, and F.-Y. Dupradeau, Automatic and highly reproducible RESP and ESP charge derivation: Application to the development of programs RED and X RED, submitted to the 227th ACS National Meeting, Anaheim, CA, March 28, April 1, 2004. http://www.u-picardie.fr/labo/lbpd/RED/.

29 NAMD was developed by the Theoretical and Computational Biophysics Group in the Beckman Institute for Advanced Science and Technology at the University of Illinois at Urbana-Champaign: L. Kal, R. Skeel, M. Bhandarkar, R. Brunner, A. Gursoy, N. Krawetz, J. Phillips, A. Shinozaki, K. Varadarajan, and K. Schulten, *J. Comput. Phys.*, **151**, 283 (1999). http://www.ks.uiuc.edu/Research/namd/.

30 H. C. Andersen, *J. Comput. Phys.*, **52**, 24 (1983).

31 T. Darden, D. York, and L. Pedersen, *J. Phys. Chem.*, **98**, 10089 (1993).

32 W. Humphrey, A. Dalke, and K. Schulten, *J. Mol. Graphics*, **14**, 33 (1996). http://www.ks.uiuc.edu/Research/vmd/.

33 P. Cieplak, J. W. Caldwell, and P. A. Kollman, *J. Comput. Chem.*, **22**, 1048 (2001). The electronic version is available at the AMBER web site: http://amber.scripps.edu/.

34 J. H. Halton, *Numer. Math.*, **2**, 84 (1960).